Total and differential cross-section calculations for proton-impact ionization of hydrogen at low energies

Shiyang Zou
Department of Fusion Science, School of Mathematical and Physical Science, the Graduate University for Advanced Studies, Oroshi-cho 322-6, Toki, Gifu 509-5292, Japan

Lukáš Pichl
Foundation of Computer Science Laboratory, University of Aizu, Tsuruga, Ikki, Aizuwakamatsu, Fukushima 965-8580, Japan

Mineo Kimura
Graduate School of Science and Engineering, Yamaguchi University, Ube, Yamaguchi 755-8611, Japan

Takako Kato
National Institute for Fusion Science, Oroshi-cho 322-6, Toki, Gifu 509-5292, Japan
(Received 21 May 2002; published 11 October 2002)

We have computed the single-differential and total ionization cross sections for the proton-hydrogen collision system at low-energy range (0.1–10 keV/amu), using the electron translation factor corrected close-coupling method. Full convergence of ionization cross sections as a function of H_2^+ molecular basis size was achieved by including up to ten bound states and 11 continuum partial waves. The present results are compared with the available experimental data and various theoretical models. Our calculated cross sections are in an excellent agreement with the recent experiments of Shah *et al.* [J. Phys. B. **31**, L757 (1998)], but decrease more rapidly than the cross sections measured by Pieksma *et al.* [Phys. Rev. Lett. **73**, 46 (1994)] with decreasing energy. We have found that the $1s\sigma_g$ electron ionization is a rather higher-level ladder climbing process than a direct mechanism; the $2p\sigma_u$ electron, on the contrary, is ionized directly and the higher levels act as a temporary trap.

DOI: 10.1103/PhysRevA.66.042707 PACS number(s): 34.50.Fa, 52.20.Hv

I. INTRODUCTION

Ion impact ionization has been an interesting problem for many years, with its important application in fusion reactors, radiation damage in biological matters, energy loss of heavy ions in solid targets, etc. There is an enormous amount of efforts to fully understand the electron emissions during ion-atom collisions from both the experimental and the theoretical perspectives (see Refs. [1–4] and references therein). Yet, our understanding of even such a basic ion-atom collision system, proton on hydrogen, is not very good especially at low energies. At keV energies, the total ionization cross sections obtained by experimental studies of Pieksma *et al.* [5] were found to be quite larger than the recent measurements of Shah *et al.* [6] below 10 keV/amu, and to decrease much less rapidly with the energy decrease. At the lowest energy considered (1 keV/amu), the cross sections of Pieksma *et al.* [5] exceed the values given by Shah *et al.* [6] by $\sim$ four times. The numbers from the precise experiments [7,8] and the extensive theories [9–11] disagree by 20% at the peak of ionization cross section. The above experimental and theoretical results are shown in Fig. 1 together with other main contributions over the years, and detailed statements on these works are given in below.

Dealing with ionization, we should always count for the probabilities of concurrent processes, i.e., elastic scattering, target excitation, and electron capture to the projectile. At low-to-intermediate energies, where the ionization is intertwined with other inelastic and elastic processes, it is not possible to describe one process accurately without treating all of them. Thus, it is a paramount to develop an approximation providing high accuracy cross sections for proton-impact ionization.

The first attempt at calculating ionization cross sections in slow *p*-H collisions was performed by SethuRaman *et al.* [12]. They employed the electron translation factor (ETF) modified molecular orbital as zero-order basis to compute the first-order couplings, and then solved the system in the perturbation approximation. It is a sensible thing to do if the cross section is small (i.e., the coupling is weak). In such an approach, they calculated the energy distributions of ejected electron at collision energies 50–500 eV, but the total ionization cross sections were not presented. Later, Thorson and co-workers [13,14] have studied extensively the base of ETF-modified molecular-orbital close-coupling approach. They presented suitable electron translation factors based on the molecular-state switching functions in order to correct the asymptotic behavior of nonadiabatic couplings. Thorson *et al.* also gave a formulation of molecular basis close-coupling expansion, in which the flux loss from the truncated basis space has been accounted for. However, the observable quantities, total ionization cross sections, are still not presented by them.

Winter and Lin [15] proposed a triple-center atomic-state expansion method for describing ionization at low energies. This method accounts for the mechanism in which the electron is not removed until it is asymptotically located at the point of unstable equilibrium between the nuclei (the third center). Further, elaboration of the triple-center atomic-orbitals method by McLaughlin *et al.* [16] showed a good

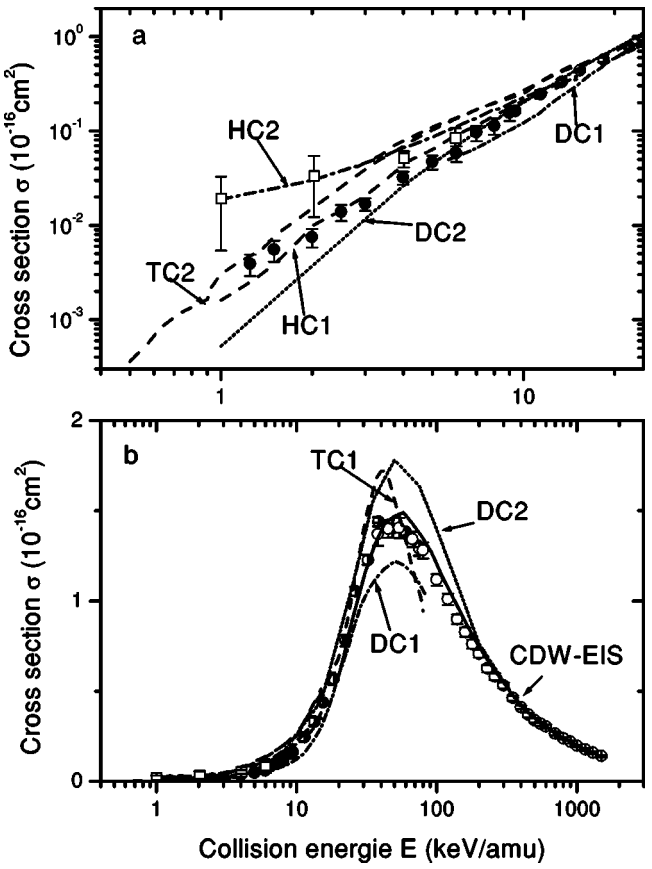

FIG. 1. Total ionization cross sections of proton-hydrogen system: panels (a) and (b) are for low- and high-energy regions, respectively. The circles with error bars show measured cross sections of Shah *et al.* [6–8]; squares with error bars show measured cross sections of Pieksma *et al.* [5]; curve HC2 shows hidden-crossing theory with *S* and *T* and radial decoupling promotion mechanisms [19]; curve HC1 shows hidden-crossing theory with only *S* and *T* promotion mechanisms [5]; curve TC2 shows close-coupling triple-center calculations of Shah *et al.* [6]; curve TC1 shows close-coupling triple-center calculations of Mclaughlin *et al.* [16]; curve DC2 shows two-center close-coupling calculations of Toshima [9]; curve DC1 shows two-center close-coupling calculations of Fritsch and Lin [17]; and curve CDW-EIS shows continuum distorted-wave eikonal initial-state approximation of Crothers and McCann [35].

agreement with the previous method of Ref. [15] for all energies considered. Both these calculations predict values larger than the experimental cross sections of Refs. [6,8], but the discrepancy is the smallest at the lowest-energy region that they considered. The values obtained by Fritsch and Lin [17] in their double-center 46 atomic-state-plus-pseudostate calculations (which were extended down to 4 keV/amu) were found to be smaller, on the contrary, they also exhibit closer agreement with the experiment in the lowest-energy region. A very detailed study of the two-center atomic-orbital expansion approach by Toshima [9] provided the ionization cross sections at the energy range 1–800 keV/amu, which were found to be 20% higher than the experiments of Shah and co-workers [7,8] at the peak of ionization cross section. But also two more recent calculations [10,11] claimed that they are in good agreement with Toshima [9] and about 20% higher than the experimental values [7,8] at the maximum. The cross sections from Toshima [9] agree well with the measured data of Ref. [6] at energies 4–10 keV/amu, but decrease more rapidly than those of Ref. [6] below 4 keV/amu.

Pieksma *et al.* [5] calculated the velocity distributions of ejected electrons and total ionization cross sections based on the hidden-crossing model with the contributions from *T*-type crossing (connected with the saddle-point ionization mechanism) and *S*-type crossing (associated with the transition from quasimolecular to united-atom behavior). In their work, the additional low-energy contributions from radial decoupling mechanism proposed by Ovchinnikov and Macek [18], which involve the decoupling of electron on nuclear motion within the united-atom limit, were also considered. At that time, the calculations of Pieksma *et al.* came below the available experimental data [5] and decreased more rapidly with the decreasing energy. Later, the contributions of radial decoupling mechanism were recalculated in a recent paper of Pieksma *et al.* [19]. The new values include the contributions from this recalculated radial decoupling mechanism, and therefore they are in a better agreement with the experimental values of Ref. [5], but disagree with the more recent experimental data by Shah *et al.* [6]. The cross-section data in Ref. [6] decrease much more rapidly than those of Pieksma *et al.*, both for the calculated [19] and the measured [5] values, but agree well with the older version of hidden-crossing calculations [5].

On the experimental side, the *p*-H system is difficult for investigation because of problems in making and characterizing the atomic hydrogen target. At low energies, the difficulty also comes from making high current and low velocity protons. The first studies by Fite *et al.* [20] measured the ionization cross section at 0.04–40 keV/amu, and the results were found to be of higher magnitude than the generally accepted data of Ref. [8]. Experimental studies by Pieksma *et al.* [5], focusing on the identification of saddle-point electrons, produced the total ionization cross sections at 1–6 keV/amu, which were found to follow a v^2 dependence on the collision velocity near the threshold [19]. The error bar is the largest at the lowest energy of 1 keV/amu for the cross-section measurement of Ref. [5]. At the low keV energies, the most recent measurements on ionization in *p*-H collisions were carried out by Shah *et al.* [6] in the range 1.25–9 keV/amu. They obtained the absolute values of total ionization cross sections with the accuracy in the range 20–30 %. The cross sections of Shah are 45% smaller than those of Ref. [5] at 6 keV/amu and they decrease much more rapidly, which results in the difference from the values of Ref. [5] as high as the factor of ~ 5 at the lowest energies considered.

On the theoretical side, the *p*-H system is especially interesting because it provides a prototype within which a variety of important physical and methodological problems can be studied in a well-defined manner. Molecular basis expansions are widely recognized as an appropriate theoretical approach to the slow ion-atom collisions. However, molecular-state calculations require careful consideration of the effects of ETF's [1,13,21]. Neglect of these introduces spurious long-range couplings and can also lead to incorrect physical

predictions [1,13,21]. In this work, the ETF's appropriate for molecular states, with the two-center character, are derived by using the method of switching functions. The well-defined switching functions for the exact molecular states of H_2^+ have been deduced by an analytical two-center decomposition scheme by Thorson *et al.* [22], and used to deal with the charge transfer and the excitation resulting in very good results [23]; we have adopted these analytical switching functions in our calculations.

In the light of the above discussion, we have calculated the differential cross sections (DICS's) and the total cross sections (TICS's) for ionization of atomic hydrogen by proton impact at low collision energy range 0.1–10 keV/amu, including the charge transfer and the excitation channels into consideration. The present paper is organized as follows. For the sake of completeness and self-consistency, in Sec. II we describe the theoretical model in an extent necessary for understanding the method. The general theory can be found in the publications of Thorson and co-workers [13,14]. The results of our calculations are given in Sec. III, where we also compare to the available experimental values of Refs. [5,6], and to other existing theoretical results. The conclusions of our study are drawn in Sec. IV, along with our final remarks.

II. THEORETICAL METHOD

A. Molecular-orbital coupled equations

Let us assume the relative motion of the nuclei to be described classically by a vector $\vec{R}(t)$, and solve the resulting time-dependent Schrödinger equation for the electron system with Hamiltonian H_{el},

$$i\hbar \frac{d}{dt}\Psi(\vec{r},t)=H_{el}(\vec{r},\vec{R}(t))\Psi(\vec{r},t). \tag{1}$$

We expand the state vector Ψ in an ETF-modified molecular basis set, and integrate over electron coordinates $\vec{r}$. Then for the expansion coefficients $a_n(t)$ in the molecular-orbital close-coupling (MOCC) method, one obtains the coupled equations (up to the first order in velocity $\vec{v}$)

$$i\hbar \frac{da_k(t)}{dt}=\sum_{n\neq k}[\dot{R}(P^R+A^R)+R\dot{\theta}(P^\theta+A^\theta)]_{kn} \times a_n(t)\exp\left[-\frac{i}{\hbar}\int^t(\epsilon_n(t')-\epsilon_k(t'))dt'\right], \tag{2}$$

with $\Theta=\angle(\vec{v},\vec{R})$, where the usual coupling terms P,

$$P^R_{kn}=-i\hbar(\epsilon_n-\epsilon_k)^{-1}\langle\phi_k|\left[\frac{\partial H_{el}}{\partial R}\right]_{\vec{r}}|\phi_n\rangle, \tag{3}$$

$$P^\theta=-R^{-1}\langle\phi_k|\hat{L}_y|\phi_n\rangle, \tag{4}$$

are corrected by the radial and angular ETF terms,

$$A^R_{kn}=im/\hbar(\epsilon_k-\epsilon_n)\langle\phi_k|zf_n(\vec{r};\vec{R})|\phi_n\rangle, \tag{5}$$

$$A^\theta_{kn}=im/\hbar(\epsilon_k-\epsilon_n)\langle\phi_k|xf_n(\vec{r};\vec{R})|\phi_n\rangle. \tag{6}$$

Here, m is the reduced electron mass, $\hat{L}$ is the electronic orbital angular momentum, and $\vec{r}=(x,y,z)$, with z being parallel to $\vec{R}$. The switching functions $f_n(\vec{r};\vec{R})$, which describe the correlation of electron motion on nuclei, in general, depend on the molecular-state wave function $\phi_n(\vec{r},\vec{R})$. We have employed the switching function, derived by Thorson *et al.* [22] for the H_2^+ system, based on the analytical two-center decomposition of exact wave functions. All these coupling matrix elements are evaluated using Gauss-Legendre and Gauss-Laguerre quadratures with relative errors $\leqslant 1\times10^{-8}$.

Before we move on to solve the close-coupled equations (2), a subtle point associated with the ETF's modified molecular-orbital expansion approach needs to be discussed. This is the non-Hermitian Hamiltonian matrix $(\vec{P}+\vec{A})$ in Eq. (2). In any calculation, we need to replace the full Hilbert space spanned by the true discrete and continuum states with a truncated subspace. As a result, certain operators in the equations of motion cannot be fully represented, and unless great care is taken they may not even be accurately represented within the truncated subspace. This is true, in particular, for the propagator itself. Thus, a theory should consider the flux loss from the truncated subspace, and then, in contrast with the exact close-coupled equations; these equations for the wave function in the truncated subspace are necessarily nonunitary, i.e., they should not conserve probabilities. Our locally non-Hermitian Hamiltonian matrix $(\vec{P}+\vec{A})$ allows us to consider the escape of electron from the subspace spanned by the truncated basis. Importantly, the flux loss effects decrease as the basis size increases, and the probability conservation is satisfied approximately on a sufficiently large basis set. By implementing the ETF's, the basis sets of relatively small size can be considered as complete with sufficient accuracy. In the present study, we find the probability conservation is better than 1×10^{-3} with a basis set including ten bound states and 11 continuum partial waves.

Next, we briefly summarize the computation of matrix elements in Eqs. (3)–(6). H_2^+ is a prototype one-electron two-nuclei system that is separable in the conventional prolate spheroidal coordinates $\vec{r}=(\xi,\eta,\phi)$, and the corresponding eigenvalues ϵ_k and wave functions $\phi_k(\vec{r};R)$ can be calculated with great numerical accuracy [24–30].

The wave function is factored out

$$\phi_k(\xi,\eta,\varphi;R)=C_k(R)\Lambda_k(\xi,R)M_k(\eta,R)e^{i\mu\varphi}, \tag{7}$$

where $C_k(R)$ is a normalization constant, and functions $\Lambda_k(\xi,R)$ and $M_k(\eta,R)$ describe the quasiradial and quasiangular motions of electron, respectively. The index μ labels the component of electronic angular momentum on the $\vec{R}$ axis. The letter k stands for the three quantum numbers E, μ, and A (A is equivalent to the orbital angular momentum for $R=0$). The one-dimensional wave functions in Eq. (7) are found in semianalytical forms, and the coupling terms in

Eqs. (3)–(6) are then readily computed. The details of the method can be found in the Refs. [24–30].

B. Perturbative and nonperturbative solutions

The close-coupled equations [Eq. (2)], can be solved by numerical integration in full dimension, but also possibly using a perturbation approach. Accounting for the fact that all the discrete-continuum couplings are very weak (see Sec. III A), we could thus construct a faster algorithm for ionization problems.

Let us now consider a system that contains n-bound states plus one continuum state, then the time-dependent Schrödinger equations for $(n+1)$ channels reads,

$$i\hbar\begin{pmatrix}\dot{a}_1\\ \dot{a}_2\\ \vdots\\ \dot{a}_n\\ \dot{\alpha}_\epsilon\end{pmatrix}=\begin{pmatrix}0 & C_{12}(t) & \cdots & C_{1n}(t) & \aleph_{1\epsilon}(t)\\ C_{21}(t) & 0 & \cdots & C_{2n}(t) & \aleph_{2\epsilon}(t)\\ \vdots & \vdots & \ddots & \vdots & \vdots\\ C_{n1}(t) & C_{n2}(t) & \cdots & 0 & \aleph_{n\epsilon}(t)\\ \aleph_{\epsilon 1}(t) & \aleph_{\epsilon 2}(t) & \cdots & \aleph_{\epsilon n}(t) & 0\end{pmatrix}\times\begin{pmatrix}a_1\\ a_2\\ \vdots\\ a_n\\ \alpha_\epsilon\end{pmatrix}, \tag{8}$$

where α_ϵ is the ionization amplitude and ϵ stands for the continuum state energy. Matrix elements $\aleph_{\epsilon i}(t)$ are

$$\aleph_{\epsilon i}(t)=\kappa_{\epsilon i}(t)\exp\left[-\frac{i}{\hbar}\int_{-t_0}^{t}(\epsilon_i(t')-\epsilon)dt'\right],$$

where $\kappa_{\epsilon i}(t)$ denotes the coupling from ith bound state to continuum ϵ. Suppose the ionization probability is small, we then solve Eq. (8) in a first-order perturbation approximation for transition amplitudes. Finding first the $n\times n$ bound state solutions $a_i(t)$, we see that

$$\alpha_\epsilon(t_0)\simeq\sum_{i=1}^{n}\int_{-t_0}^{t_0}\kappa_{\epsilon i}(t)\times\exp\left[-\frac{i}{\hbar}\int_{-t_0}^{t}(\epsilon_i(t')-\epsilon)dt'\right]a_i(t)dt. \tag{9}$$

The phase factor above rapidly oscillates with t, which makes the results small and the method of Eq. (9) applicable. Hence we can calculate at once the ionization cross sections for whole energy distribution ϵ of ejected electron, changing only the couplings $\kappa_{\epsilon i}(t)$. In general, the method of Eq. (9) is $\sim$100 times faster than that of solving the differential Eq. (8).

Although the perturbation solutions reproduce the final-state amplitudes much faster, it should be noted that the accuracy decreases with the increasing ionization probability. In a collision with $E>5$ keV/amu, $\epsilon<0.1$ Ry, and $b\sim 0.5$, the ionization probability can be higher than 0.1 even 0.2 in some cases. Since integration of differential equations (2) in our case is tractable, we prefer to solve Eq. (2) directly to ensure that no important interactions are missing. A Runge-Kutta-Vener method with 10^{-6} accuracy has been employed in the present study to keep the overall numerical inaccuracy confined to the cross sections smaller than 10^{-3} after integrating the transition probabilities over all impact parameters.

Since the collision Hamiltonian is rigorously centrosymmetric for p-H system, the state vector Ψ in Eq. (1) is composed of noninteracting g (gerade) and u (ungerade) components, and thus there are corresponding sets of g and u close-coupled equations (2). If index "1" designates the initial states in each set ($1s\sigma_g$ or $2p\sigma_u$, respectively), then the initial conditions for Eq. (2) (corresponding to "proton A plus atom B") is

$$a_k(t=-\infty)=1/\sqrt{2}\,\delta_{1k}, \tag{10}$$

and (for given energy E and each impact parameters b) the final-state amplitudes $a_k(E,b)$ are computed.

Once the final-state amplitude $a_k(t=+\infty)$ is known, we can define the probability of excitation/or ionization to the molecular state k as

$$P_k(E,b)=|a_k(t=+\infty)|^2, \tag{11}$$

and the corresponding individual cross section is

$$Q_k(E)=2\pi\int P_k(E,b)bdb. \tag{12}$$

In ionization problems, $Q_k(E)$ is the partial ionization cross section, labeled by ϵ, λ, and μ. Hence the differential ionization cross section is determined by summing $Q(\epsilon,\lambda,\mu;E)$ over quantum numbers λ, μ;

$$\frac{d\sigma}{d\epsilon}=\sum_{\lambda,\mu}Q(\epsilon,\lambda,\mu;E) \tag{13}$$

and the total ionization cross section

$$\sigma=\int\frac{d\sigma}{d\epsilon}d\epsilon \tag{14}$$

is obtained by integrating the energy distribution of the ejected electrons.

III. RESULTS AND DISCUSSION

To compute the ionization cross sections, we have done systematic calculations with basis sets A, B, and C, as listed in Table I. Comparing the numerical results with different basis sets allows us to study the convergence of ionization cross sections with the basis size. In addition, some selected calculation have been done on the ungerade component of basis set C without $2p\pi_u$ (set D) to understand the role of upper levels in the ionization dynamics. The continuum component is common in the basis sets A (direct ionization), B, C

TABLE I. Molecular basis sets for systematic close-coupling calculations.

Sets	Gerade basis states	Ungerade basis states	Number of all states
Continuum	$\|\epsilon s\sigma_g\rangle$	$\|\epsilon p\sigma_u\rangle$, $\|\epsilon p\pi_u\rangle$	
	$\|\epsilon d\sigma_g\rangle$, $\|\epsilon d\pi_g\rangle$	$\|\epsilon f\sigma_u\rangle$, $\|\epsilon f\pi_u\rangle$	
	$\|\epsilon g\sigma_g\rangle$, $\|\epsilon g\pi_g\rangle$	$\|\epsilon h\sigma_u\rangle$, $\|\epsilon h\pi_u\rangle$	
	Five partial waves, for 32 energies	Six partial waves, for 32 energies	11×32 $=352$
and bound	All above, plus	All above, plus	
A	$\|1s\sigma_g\rangle$	$\|2p\sigma_u\rangle$	354
B	All above, plus	All above, plus	
	$\|3d\pi_g\rangle$	$\|2p\pi_u\rangle$	
	$\|3d\sigma_g\rangle$	$\|3p\sigma_u\rangle$	
	$\|2s\sigma_g\rangle$	$\|3p\pi_u\rangle$	360
C	All above, plus	All above, plus	
	$\|4d\pi_g\rangle$	$\|4f\sigma_u\rangle$	362
D		All above, minus	
		$\|2p\pi_u\rangle$	196

[a]Set *D* contains four discrete states ($2p\sigma_u$, $3p\sigma_u$, $3p\pi_u$, $4f\sigma_u$) and 192 continuum states (32 energies for the six *u*-partial waves above).

(indirect ionization), and *D*, which contains 32 energies below 1.0 Ry for each partial wave [31]; then the total continuum states are accounted for up to 352. Within the straight line approximation, we have solved the coupled differential equations, [Eq. (2)], for 100 impact parameters arranged in 0.0–6.0 a.u. at 32 collision energies from 0.1–10 keV/amu.

A. Couplings and ionization probabilities

Employing the ETF's of Ref. [22], we have computed the nonadiabatic coupling for both discrete-to-discrete and discrete-to-continuum transitions. The corrections arising from ETF's exactly cancel the spurious asymptotic couplings and produce substantial reductions in the size and effective range of most coupling matrix elements. Since the discrete-discrete couplings have been discussed in detail by Kimura and Thorson [23], we only show the discrete-continuum couplings in this paper.

The ETF-corrected couplings from $1s\sigma_g$ and $2p\sigma_u$ to the lowest partial waves are plotted in Figs. 2 and 3 for the ejected electron energies $\epsilon=0.01$ and 1.0 Ry, respectively. It can be seen that the corrected couplings are significant only for the first two or three partial waves and their range is less than 10 a.u. Whereas the uncorrected perturbed stationary-state (PSS) theory predicts large couplings to 30–40 continuum and an envelope of PSS couplings that has a range of 40 a.u.(see also Ref. [32]). The strongest coupling from $2p\sigma_u$ is $\langle 2p\sigma_u|\mathrm{H(ang)}|\epsilon p\pi\rangle$ caused by rotation of the quasimolecule, and it exceeds the radial coupling of $2p\sigma_u$,

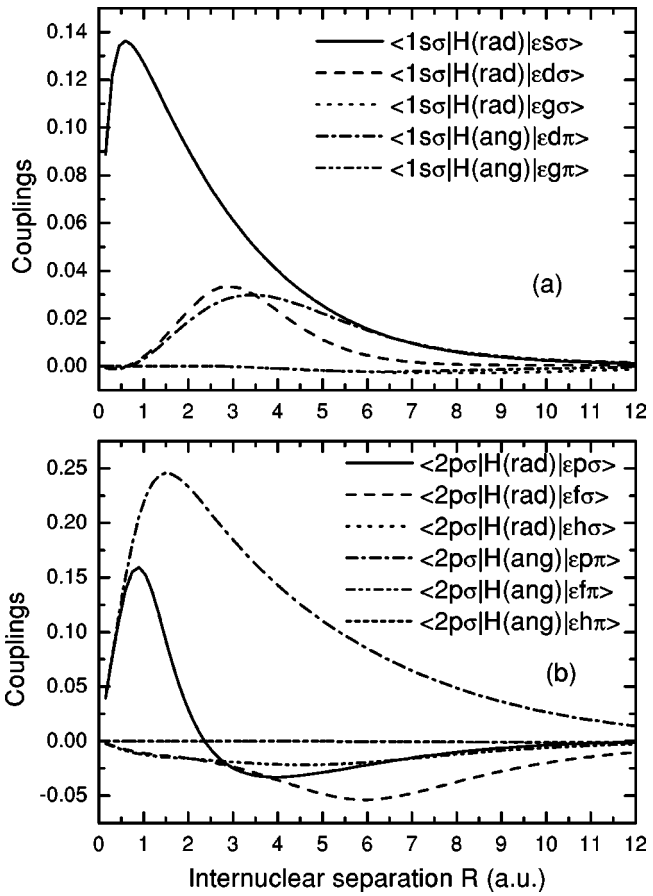

FIG. 2. Couplings to the lowest partial waves for final electron energies $\epsilon=0.01$ Ry from the $1s\sigma_g$(panel a) and $2p\sigma_u$(panel b) states in H_2^+ molecule, where H(rad) and H(ang) are the radial and angular coupling operators with ETF corrections added, respectively.

$\langle 2p\sigma_u|\mathrm{H(rad)}|\epsilon p\sigma\rangle$ by 40% at the maximum. However, for the $1s\sigma_g$ coupling, $\langle 1s\sigma_g|\mathrm{H(rad)}|\epsilon s\sigma\rangle$ also dominates the other couplings from $1s\sigma_g$.

Figure 4 shows the energy dependence of couplings $\langle 1s\sigma_g|\mathrm{H(rad)}|\epsilon s\sigma\rangle$ and $\langle 2p\sigma_u|\mathrm{H(rad)}|\epsilon p\sigma\rangle$. The couplings from $2p\sigma_u$ are much sensitively dependent on the energy of continua electron than those from $1s\sigma_g$; the size of couplings from $2p\sigma_u$ is reduced by about factor of 2 with the continua electron energy increase from 0.01 Ry to 1.0 Ry; however, couplings from $1s\sigma_g$ are changed only by $\sim$25% in size, (see also Figs. 2 and 3). The sensitive energy dependence of couplings from $2p\sigma_u$ is understood by the potential curve of $2p\sigma_u$: near the united-atom limit, $2p\sigma_u$ lies about 1.0 Ry below the ionization limit, in contrast to the 4.0 Ry deep potential of $1s\sigma_g$. Then the change of couplings in size is analogous to the potential curves of bound states, as indicated in Eq. (3).

Referring to Figs. 2, 3, and 4, we have said that ETF's simultaneously and systematically reduce the couplings from discrete state to all continuum states, and the couplings are significant only for small internuclear separations. Considering the potential curves of $1s\sigma_g$, $2p\sigma_u$ and the corresponding couplings, we may predict tentatively without detailed

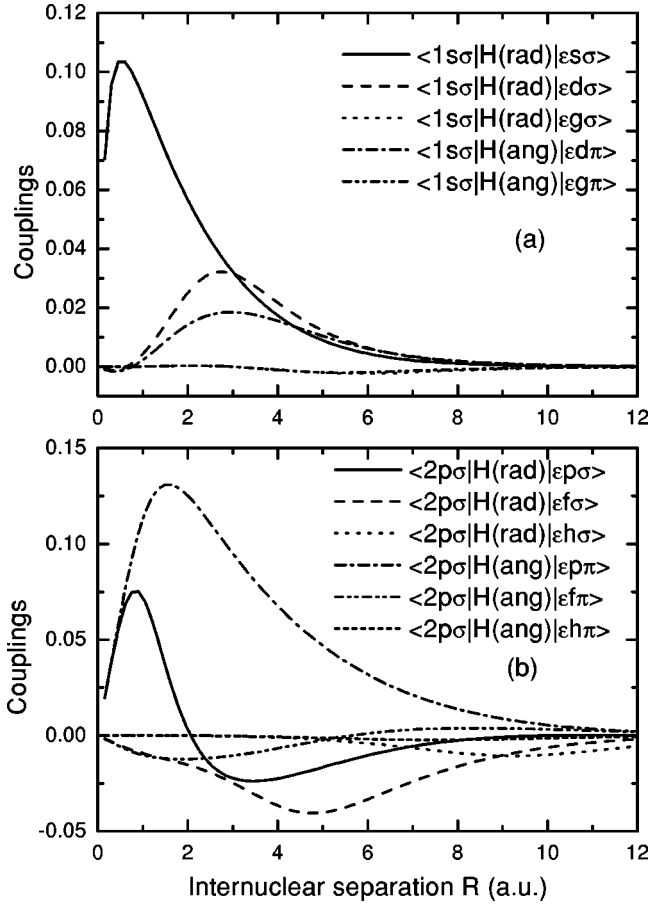

FIG. 3. Same as Fig. 2 except $\epsilon = 1.0$ Ry.

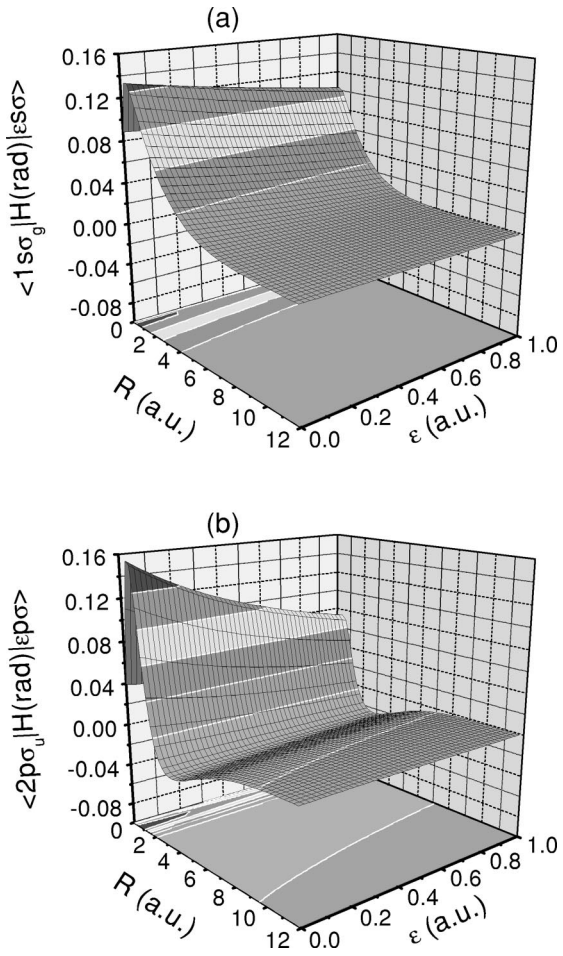

FIG. 4. Energy dependence of ETF-modified couplings $\langle 1s\sigma_g|\mathrm{H(rad)}|\epsilon s\sigma\rangle$: upper panel, and $\langle 2p\sigma_u|\mathrm{H(rad)}|\epsilon p\sigma\rangle$: lower panel.

numerical calculations: (i) ionization cross sections of $2p\sigma_u$ electrons are much larger than those of $1s\sigma_g$ electrons, (ii) ionization is mainly caused by close collisions.

Collision history (molecular-state probability vs times) of $p\sigma$ and $p\pi$ ionization channels are shown in Fig. 5 at collision energy $E=2$ keV/amu for impact parameter $b=1.0$ a.u. and final electron energy $\epsilon=0.01$ Ry. The state probabilities $P(b)$ oscillate with collision time vt which shows the electron transition in molecular states. The magnitude of oscillation decreases with vt increasing and becomes stable after propagating a sufficiently long period. Ionization probabilities with basis set *A* are higher than those of basis set *C* by $\sim 30\%$ in $p\sigma$ channel, and by one order of magnitude in $p\pi$ channel. It is due to the important flux loss from $2p\sigma_u$ to $2p\pi_u$. The two states $2p\sigma_u$, $2p\pi_u$ are degenerated in the united-atom limit and strongly coupled by the rotation of quasimolecule. Since couplings to continuum states are significant only for small internuclear separation *R*, an excitation to $2p\pi_u$ does not reduce the energy gap to continuum much. Thus the strong angular coupling $\langle 2p\sigma_u|\mathrm{H(ang)}|2p\pi_u\rangle$ efficiently depopulates the initial state $2p\sigma_u$ and eliminates the maximum appearing in set *A* near $vt=3.5$ a.u. To confirm this point, a calculation is done on the basis set *D* in which $2p\pi_u$ has been removed, and the results are shown as dash dotted lines in this figure. We can see that the upper levels except $2p\pi_u$ increase the ionization probability to $p\sigma$ channel by $\sim 25\%$ and decrease the ionization in $p\pi$ channel by $\sim 40\%$ comparing to set *A*. However, $2p\pi_u$ produces much stronger effect than all the others. Fig. 5, we also plot the ionization probabilities with the basis set *B*, which is difficult to distinguish from values of set *C* by eyes. It means that the calculations are already converged with the basis set including five bound states and six continuum partial waves for ungerade component at the low keV energies.

Figures 6 and 7 show the weighted ionization probabilities $P(b)b$ of *u* components as a function the impact parameter *b* at the ejected electron energies $\epsilon=0.01$, 0.1, and 1.0 Ry with the collision energies $E=2$ and 4 keV/amu, respectively. The area below each curve is proportional to the value of partial cross section. From these two figures, it can been seen that only $p\sigma$ or $p\pi$ channel is important for electron emission in this energy range. The ionization probabilities decrease rapidly with the increasing ejected electron energy and with the decreasing collision energy. With the ejected electron energy increasing from 0.1 Ry to 1.0 Ry, the ionization probabilities drop down by one order of magnitude at the maximum of $bP(b)$ for collision energies $E=2$ or 4 keV/amu. Peak of ionization probabilities shifts to the left-hand side (i.e., to small impact parameters) with continua

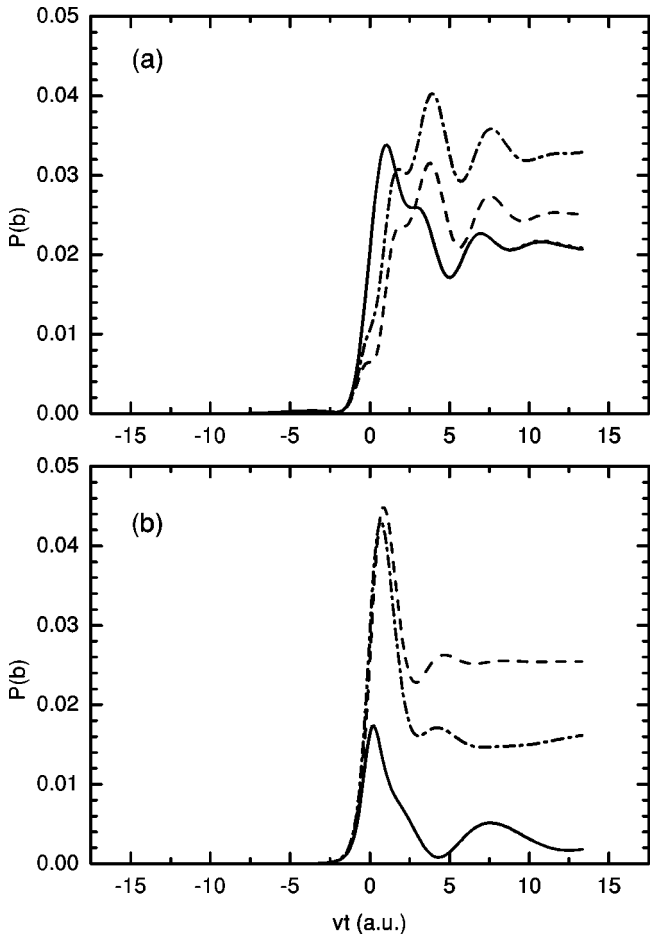

FIG. 5. Collision history [molecular-state probabilities vs weighted time $(v\times t)$] for the $p\sigma$ (upper panel) and $p\pi$ (lower panel) ionization channels. Collision energy is $E=2$ keV/amu, impact parameter $b=1.0$ a.u, and the ejected electron energy $\epsilon=0.01$ Ry. Dashed lines show basis set *A*; dotted lines show set *B*; solid lines show set *C*; and dash dotted lines, show set *D*.

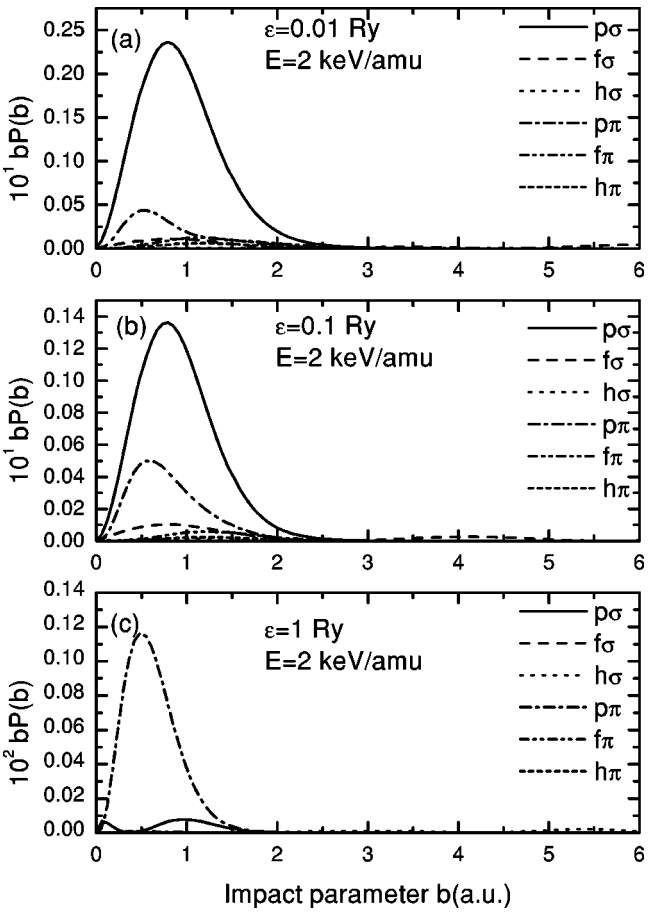

FIG. 6. Weighted ionization probabilities as a function of the impact parameter b (atomic units) at the collision energy of 2 keV/amu. The three figures are for the ejected electron energies $\epsilon=0.01$, 0.1, and 1 Ry from top to bottom. Calculations are performed on the basis set *C*.

electron energy increasing. In the top panel in Fig. 6 or Fig. 7, $\epsilon=0.01$ Ry and ionization to $p\sigma$ channel predominates others, while at the bottom panel, $\epsilon=1.0$ Ry and the $p\pi$ channel is the most important. It should also be noted that distribution of ionization probabilities in channels depends on the collision energy E; $p\pi$ electron ionization probability is order of magnitude higher than that of $p\sigma$ at $E=2$ keV/amu and by factor of 2 at $E=4$ keV/amu. At low keV energies, the ionization mainly produces slow electrons in $p\sigma$ channel by the relative long-range interactions, while the fast electron can only be produced by the close collision through the angular coupling mechanism as shown in the bottom panel of Figs. 6 and 7. The fast free electrons are in π states.

The distribution of ionization probability $bP(b,E)$ is shown in Fig. 8 as a function of ejected electron velocity v_e and impact parameter b for a collision energy $E=4$ keV/amu. It can be seen that the $bP(b,E)$ peaks at $v_e\simeq 0.31$ a.u, $b\simeq 1$ a.u. and decreases rapidly with the increasing impact parameter b and final electron velocity v_e. The ionization probabilities are negligibly small for $b>3$ a.u., and most of electron emissions take place as a results of close collisions with $b\sim 1$ a.u. The distribution of ejected electron is antisymmetric, a fast electron tail at $v_e\sim 1$ a.u. is found, which is produced by and only by collisions with $b\sim 1$ a.u. Let us note at the moment that the mean radius of hydrogen atom is 1.0 a.u. and the half of collision velocity is about $V_p/2=0.28$ a.u. at $E=4$ keV/amu. Thus the ionization is mainly caused by ''head on'' (on electron) collisions and results a free electron with half of the collision velocity, i.e., $v_e\simeq V_p/2$.

For a collision energy $E=10$ keV/amu, we have plotted the ionization probability $bP(b,E)$ against the electron velocity v_e and impact parameter b in Fig. 9. The maximum of $bP(b,E)$ is near $v_e\simeq 0.40$ a.u., $b\simeq 1.2$ a.u. on the final electron velocity and impact parameter plane. Now the half of collision velocity $V_p/2$ is about 0.45 a.u., and the ejected electron velocity v_e is sightly smaller than $V_p/2$, opposite of Fig. 8. The spectra of the electrons emitted in ion-atom collisions have been recognized with peaks corresponding to soft electrons $(v_e\simeq 0)$, electron capture to the continuum $(v_e\simeq V_p)$, binary encounter collisions $(v_e\simeq 2V_p)$, and perhaps an additional peak corresponding to the ''saddle-point'' electrons $(v_e\simeq V_p/2)$ [5,19]. Although the electron distribu-

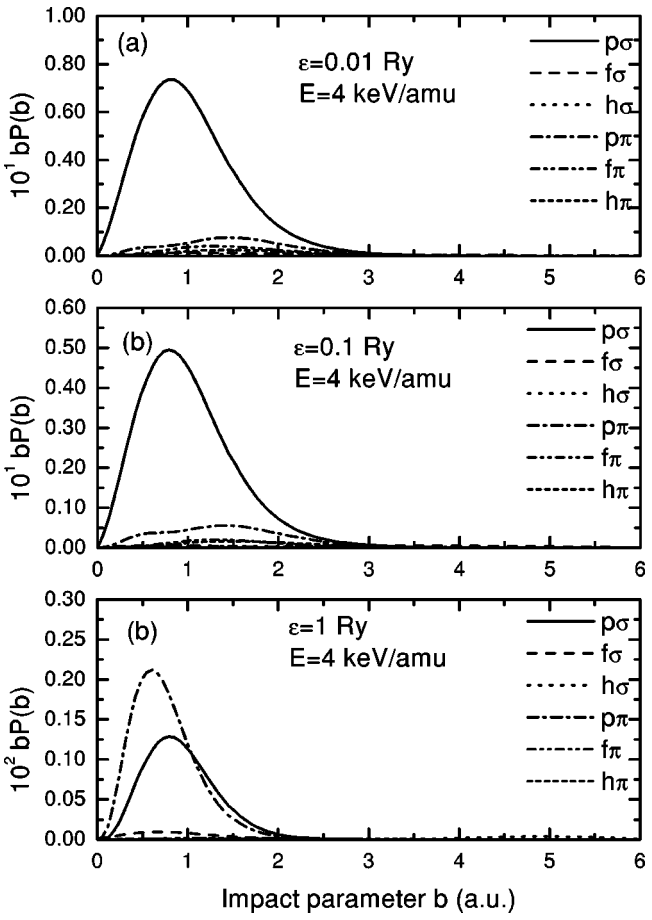

FIG. 7. Same as Fig. 6 except $E=4$ keV/amu.

tions in Figs. 8 and 9 peak near $v_e \simeq V_p/2$, there is no linear response to V_p for electron velocity v_e at the peak, say $v_e > V_p/2$ at the collision energy $E=4$ keV/amu and $v_e < V_p/2$ at $E=10$ keV/amu. Thus the maxima of ionization probabilities in Figs. 8 and 9 should not be considered as a ''saddle-point'' electron emission. With the increase in collision energy, an amount of slow electrons can be produced by a collision with large impact parameter $b \geqslant 3$, as shown in this figure. These soft electrons are in $p\pi$ state. The height of fast electron tail increases to $\sim 35\%$ of the peak, comparing to 20% in Fig. 8 at $E=4$ keV/amu.

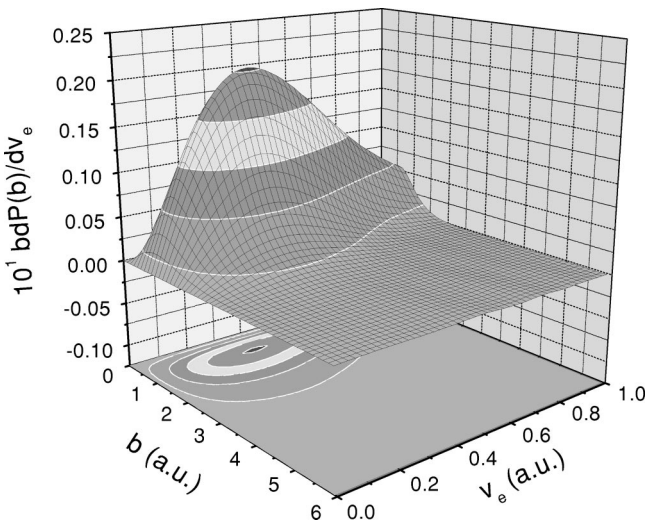

FIG. 8. Weighted ionization probability $bP(b,E)$ as a function of ejected electron velocity v_e and impact parameter b at a collision energy $E=4$ keV/amu (i.e., $V_p/2=0.28$ a.u.). In this figure, calculations are carried out with basis set *C*.

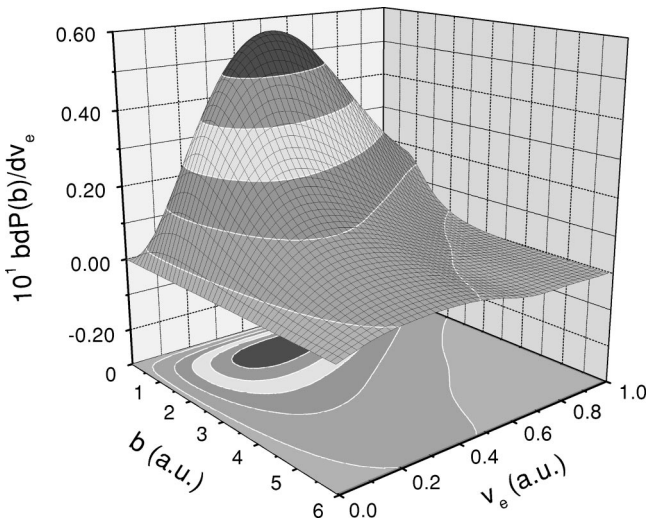

FIG. 9. Same as Fig. 8 except $E=10$ keV/amu (i.e., $V_p/2=0.45$ a.u.).

Figure 10 shows the ionization probability distribution as a function of collision velocity V_P and impact parameter b for the given final electron energy $\epsilon=0.1$ Ry, i.e., $v_e \simeq 0.32$ a.u. near the peak of $bP(b)$ in Figs. 8 and 9. The ionization probability increases with increasing collision velocity not only in the magnitude, but also in the effective range of impact parameter b. At a relatively high collision energy, electrons can be ejected by a long-range interaction,

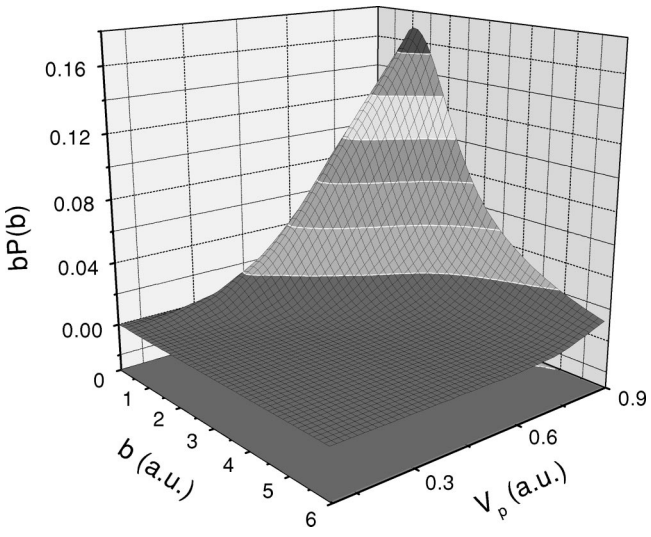

FIG. 10. Weighted ionization probabilities $bP(b,E)$ as a function of impact parameters b and collision velocities V_P. In this figure, the ejected electron energy is $\epsilon=0.1$ Ry, i.e., $v_e \simeq 0.32$ near the maximum of $bP(b,E)$ in the final electron velocity space. This calculation is performed on the basis set *C*.

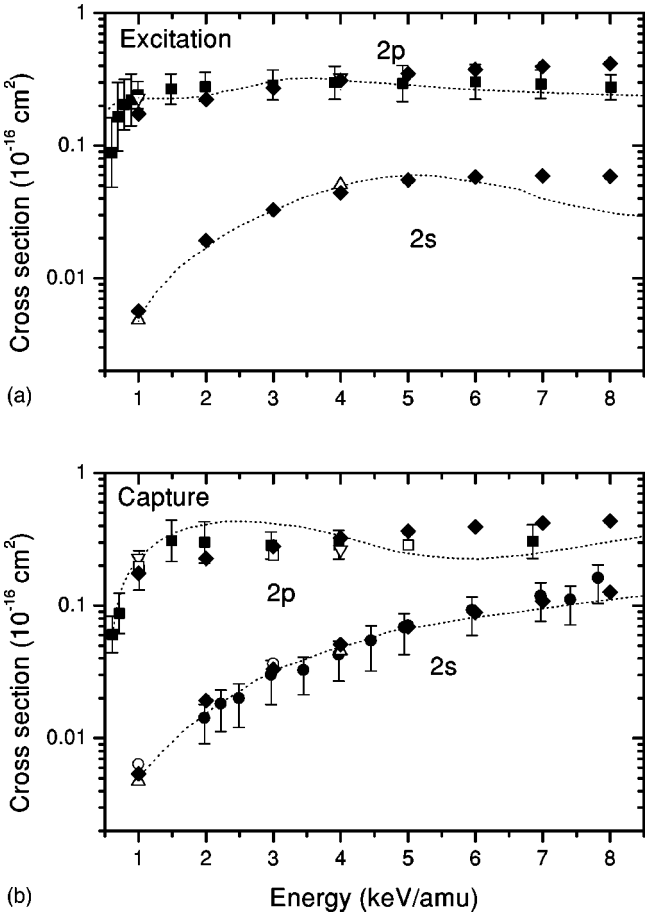

FIG. 11. Cross-section comparison (H-p system) for (a) excitation to $2s$ and $2p$ levels and (b) capture into $2s$ and $2p$ levels of atomic hydrogen in collisions with slow protons. Solid squares with error bars show measured values of Barnett [33]; solid circles with error bars show measured values of Morgan *et al.* [34]; dotted lines show the triple-center close-coupling calculations of Mclaughlin *et al.* [16]; open triangles show the double-center close-coupling calculations of Toshima [9]; open circles show molecular orbital close-coupling calculations of Kimura and Thorson [23]; and solid diamonds show present calculations with basis set *C*.

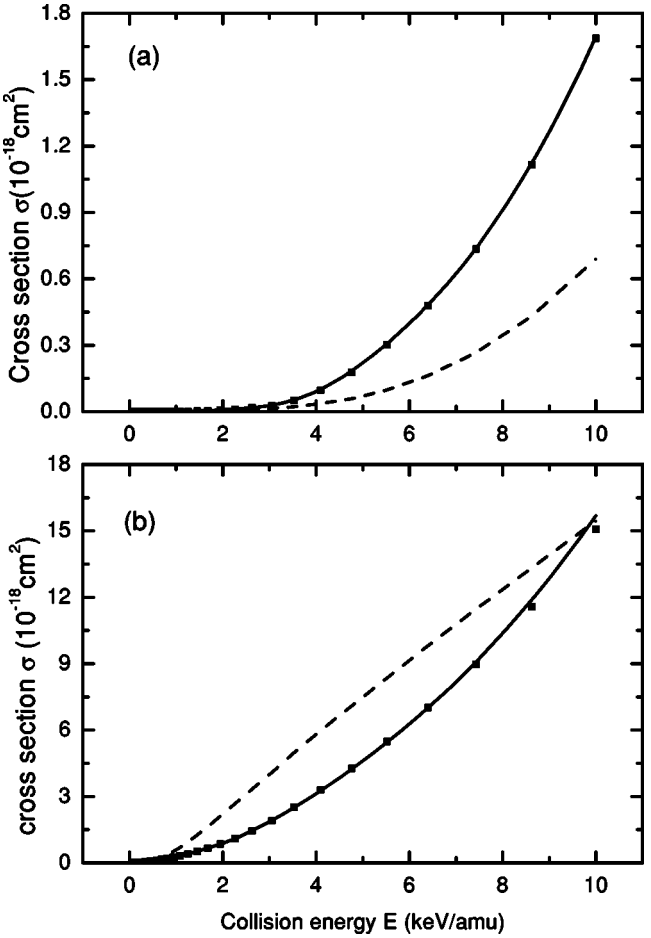

FIG. 12. Total ionization cross sections in p-H collisions: dashed lines show set *A*; solid scatters show set *B*; and solid lines show set *C*. In the figure, g components are plotted in the upper panel and u components in the lower panel.

in contrast to the slow collision emitting electrons only through ''head on'' collisions.

B. Cross sections

1. Excitation and charge-transfer cross sections

As we stated in the Introduction, target excitation and charge transfer are important processes in the collision energy range below 10 keV/amu, which may influence the hydrogen ionization cross sections. Hence we compared our results with various calculations and experiments, namely for the excitation and capture into $2s$ and $2p$ levels of atomic hydrogen in Fig. 11. Our results are in a good agreement with the measured data [33,34] for collision energies between 1 and 7 keV/amu for target excitation or capture to projectile. Yet, at higher energies, our calculated $2p$ excitation cross section increases more quickly than the measured values of Barnett [33] (cf. Fig. 11). The agreement with the double-center close-coupling calculations of Toshima [9] is better than 20% in all cases. A very good agreement for electron capture to the projectile is found in case of the previous calculations by Kimura and Thorson [23]: for instance the cross section at 5 keV in Ref. [23] agrees with our result within 5% for $2s$ charge transfer, and within 6% for $2p$ charge transfer. These are the upper bounds for all ejected electron energies; e.g., the 6% difference for $2p$ charge transfer corresponds to the ejected electron energy $\epsilon = 0.01$ Ry, and it decreases to only 1–2 % difference at $\epsilon = 1.0$ Ry.

The transitions between discrete states, which occur at large values of R in fact do cause a slower convergence of the capture/excitation cross sections. This particular case, however, does not influence our ionization cross sections, because the ETF-corrected couplings to the ionization continuum practically vanish at large values of R.

2. Ionization cross sections

The total ionization cross sections computed with the basis sets *A*, *B*, and *C* are shown in Fig. 12: g components in the upper panel, and u components in the lower panel. The corresponding ratios of TICS's with different basis set are

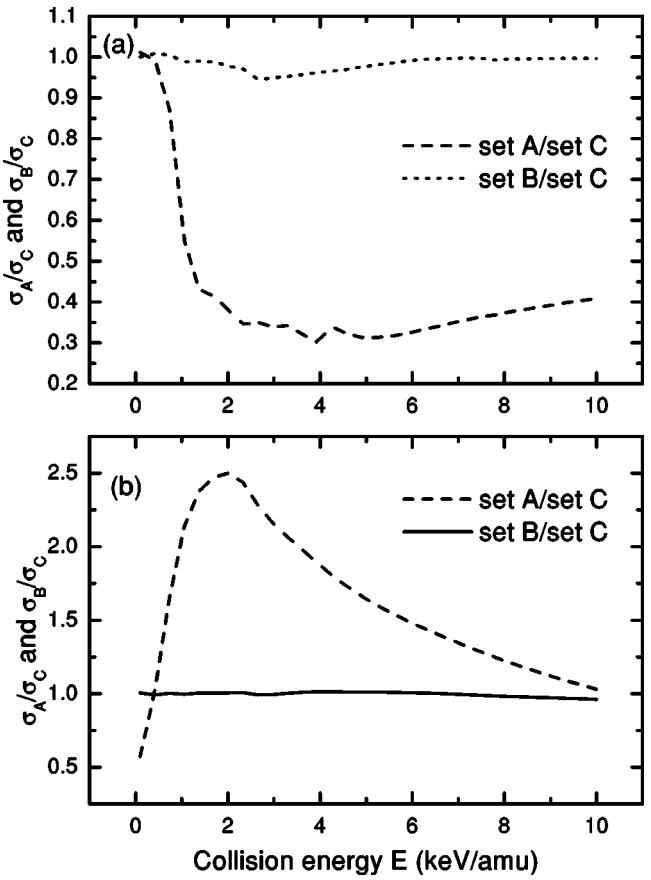

FIG. 13. Ratios of total ionization cross sections in *p*-H collisions: dashed lines show set *A* over set *C*; solid lines show set *B* over set *C*. In the figure, *g* components are plotted in the upper panel and *u* components in the lower panel.

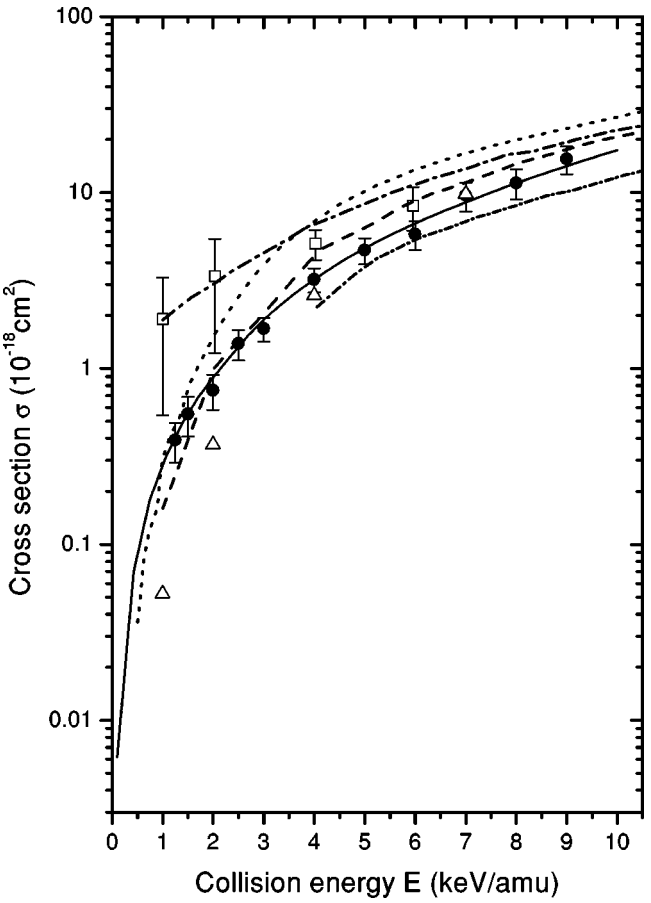

FIG. 14. Total ionization cross sections of proton-hydrogen system: solid circles show measured cross sections of Shah *et al.* [6]; open squares show measured cross section of Pieksma *et al.* [5]; dash dotted lines show hidden-crossing theory with *S* and *T* and radial decoupling promotion mechanisms [19]; dashed lines show hidden-crossing theory with only *S* and *T* promotion mechanisms [5]; dotted lines show close-coupling triple-center calculations [6]; triangles show two-center close-coupling calculations [9]; short dash dotted lines show two-center atomic-orbitals-plus-pseudostates expansion [17]; and solid lines show present ETF's modified molecular basis expansion calculations with basis set *C*.

plotted in Fig. 13. From the two figures, it is clearly seen that in case of *g* components the upper levels incorporated in basis set *C* enhance the total ionization cross sections by approximately two times at the collision energies above 2 keV/amu. This means that the dominant mechanism for ionizing a $1s\sigma_g$ electron does not involve direct excitation by a single impulse, but a ''ladder-climbing'' process in which the electron is gradually detached in a series of small impulses, and does not come out with large amounts of excess energy. However, the case of *u* components is completely different, TICS's with basis set *C* are much smaller than those of basis set *A* below 6 keV/amu at $E=2$ keV/amu with the discrepancy up to factor of 2.5. In this case, the upper levels are a trap instead of a steping stone. As stated in Sec. III A, the ionization is driven by short-range couplings and takes place only at small internuclear separations. The potential curves of bound states, especially near the united atom limit, play an essential role in interpretation of ionization dynamics. $1s\sigma$ lies far below any other bound or continuum states, but the excitation to an upper lying state significantly reduces the energy distance to the continuum, and thus effectively enhances the interaction with the continuum states. In *u* family, the strongly coupled states $2p\pi_u$ and $2p\sigma_g$ are degenerated in the united-atom limit, therefore excitation to $2p\pi_u$ does not reduce the potential much. The strong angular coupling $\langle 2p\pi_u|\mathrm{H(ang)}|2p\sigma_u\rangle$ introduces an important flux loss to $2p\sigma_u$ and decreases ionization probabilities, [see also Fig. 5]. Then the completely different roles of upper levels in ionization of *g* and *u* electrons are determined by the potential curves of bound states in H_2^+ in the united-atom limit. The difference between basis sets *B* and *C* is rather small, the ratios of TICS's differ from a unit not larger than a few percent.

Figure 14 shows the total ionization cross sections that we computed using the basis set *C* in comparison with the various theoretical calculations and the available experimental data. Our cross sections are one time smaller than those of the triple-center atomic-orbital close-coupling calculations of Ref. [6] above; they exhibit closer agreement at collision energies lower than 1.5 keV/amu. The hidden-crossing calculation including *S* and *T* promotions and the radial decoupling mechanism [19] is 30% higher than our results at 10 keV/amu. Their cross section decreases more slowly with the energy decreasing, and thus at 1 keV/amu the difference

from our calculations is as high as a factor of 6. Yet, our values are in better agreement with the hidden-crossing method including only *S* and *T* promotions [5], with the discrepancies better than 30% as usual. This holds except for the collision energy below 2 keV/amu, where the hidden-crossing calculations decrease faster, and the cross sections of Ref. [5] are by a factor of 2 smaller than the present results at 1 keV/amu. Our calculations agree well with the two-center close-coupling calculation of Toshima [9] in the range 4–10 keV/amu, but Toshima's values become smaller than us and dropped much faster below 4 keV/amu. The present results are also compared with the measurements of Pieksma *et al.* [5] and Shah *et al.* [6]. Our values come at 25% below the measured cross sections of Ref. [5] at 6 keV/amu, and decrease much more rapidly with the decreasing collision energy, the discrepancies up to a factor of 6 at lowest considered collision energy 1 keV/amu. However, our results are in an excellent agreement with the recent experimental data of Shah *et al.* [6], since they lie within the experimental error bars in the entire energy range considered. Such an agreement should be expected when the important direct and indirect ionization mechanisms are all included, boundary conditions treated properly, and the numerical accuracy of all calculations sufficiently maintained.

The total ionization cross section in *p*-H system was already plotted in Fig. 1 for a broader energy range 0.1–1000 keV/amu, in which various calculations are compared. TICS's from Toshima [9] are 20% higher than the experimental values [7,8] around $E=100$ keV/amu, and they are in a good agreement at the high-energy region. The triple-center close-coupling calculations [6,16] predicted the cross sections at low-to-intermediate energies to be larger than the measurement data [6,8] up to a factor of 2, and they decrease much faster at collision energies above 50 keV/amu. They are also found to oscillate with collision energies. The continuum distorted-wave eikonal initial-state (CDW-EIS), approximation, is a high-energy theory by Crothers and McCann [35], who obtained their cross sections in a good agreement with the measurements by Shah and co-workers [7,8] for energies above 25 keV/amu. All the above theories predicted TICS's decreasing much more rapidly than our results and the experimental data [6] below 1.5 keV/amu.

The accurate total ionization cross sections by the ETF-modified close-coupling expansion in Fig. 14 is not the only principal result of our paper. In Fig. 15, we plot the single-differential cross sections as a function of ejected electron energies ϵ and collision energies *E*. The cross sections of *g* and *u* components are shown in the upper and lower panels, respectively. The ionization cross section decreases rapidly with the increasing final electron energy and decreasing collision energy. The ionization is significant only when collision energies *E* is above 3 keV/amu for *g* components and 1 keV/amu for *u* components. At a collision energy $E=10$ keV/amu, the differential cross sections of $\epsilon=0.01$ Ry is about two orders of magnitude greater than that of $\epsilon=1.0$ Ry. The differential cross section $d\sigma/d\epsilon$ of *u* components is about one order of magnitude greater than that of *g* components at their maxima. We have projected the differential cross sections $d\sigma/d\epsilon$ on the bottom plane in this figure. There is a region in the two projections where for a constant $d\sigma/d\epsilon$, the ratio of ϵ/E is a constant. It shows that a small amount of electrons gain energies from incident protons in a single impulse, and comes out with large excess energy. Such a process is analogous to electron capture to continuum, in which the projectile transfers a part of its kinetic energy to the target in a constant rate and results free electron with $v_e \sim V_p$.

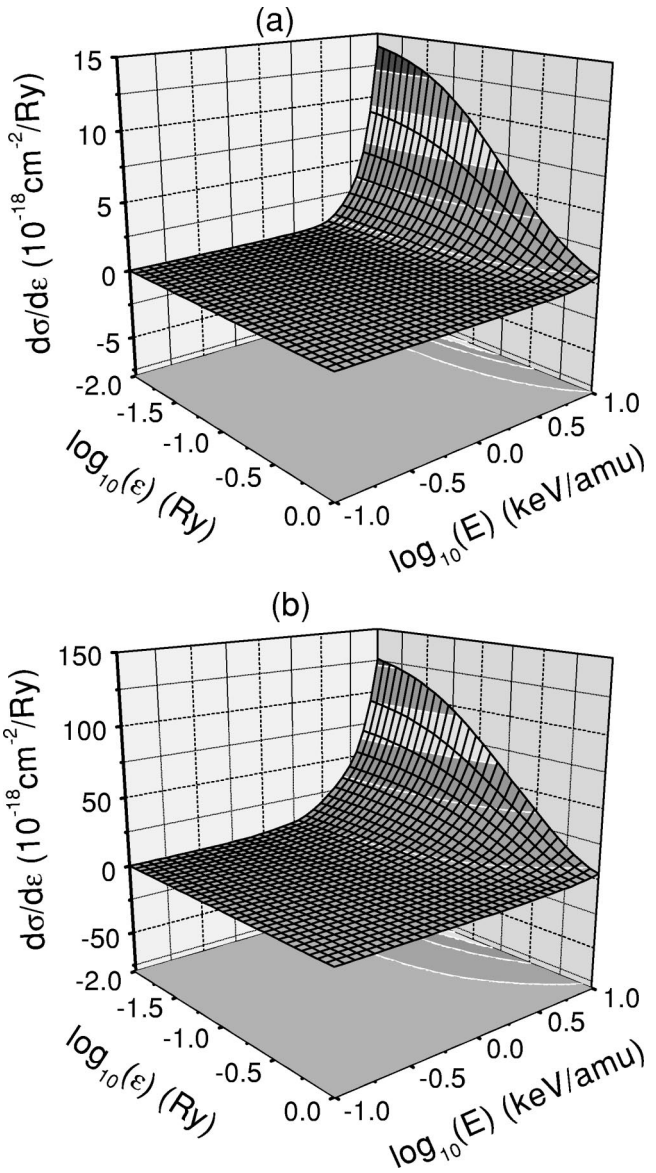

FIG. 15. Single-differential ionization cross sections of proton-hydrogen system: the *g* and *u* components are shown in the upper and lower panels, respectively. Numerical values are obtained by present ETF-modified molecular close-coupling calculations with basis set *C*.

Figure 16 shows the distribution of partial ionization cross sections as a function of collision energy. The energy of ejected electron is taken as $\epsilon=0.01$ Ry. This figure represents our previous statement that the ionization cross sections are significant only for two or three channels either for *g* components or for *u* components. In case of *g* components, $s\sigma$, $d\sigma$, and $d\pi$ are the important channels below 4 keV/

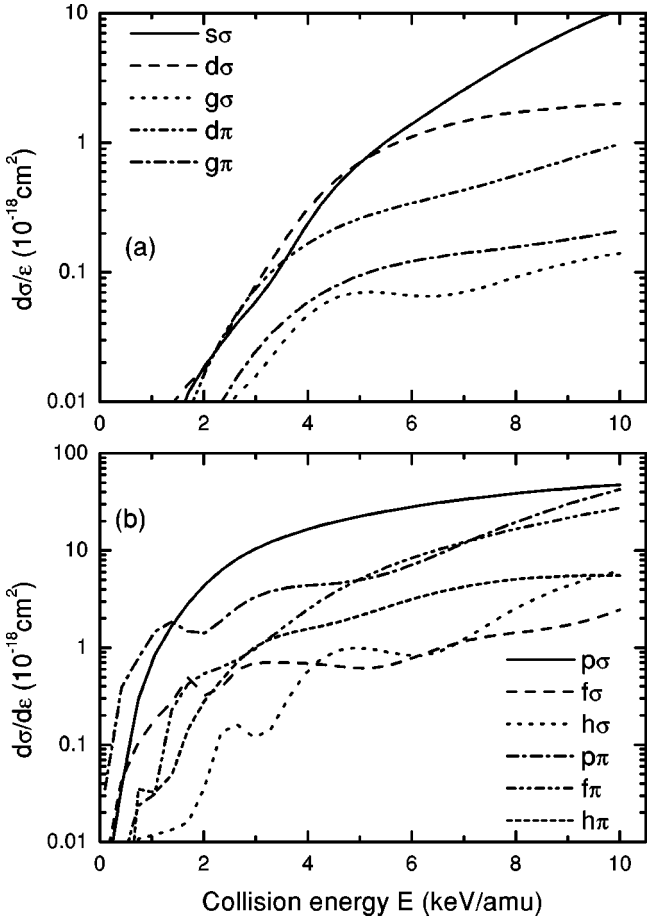

FIG. 16. Partial ionization cross sections as a function of the collision energy E for the ejected electron energy $\epsilon = 0.01$ Ry. Upper panel: g components, lower panel: u components.

amu, but the partial ionization cross sections of $s\sigma$ channels increase much more rapidly than the other two, and exceed them by order of magnitude at $E = 10$ keV/amu. The channels $p\sigma$, $p\pi$, and $f\pi$ are important in the case of u components, and the partial ionization cross sections of $p\pi$ and $p\sigma$ are almost the same at the highest energy considered i.e., 10 keV/amu.

IV. CONCLUSION

In this paper, we have provided accurate single-differential and total ionization cross sections on proton-hydrogen collision system at 0.1–10 keV/amu. We use the close-coupling expansion with ETF's modified H_2^+ molecular states. It is the first calculation using this method for the ionization problem, based on the direct evaluation of all couplings between the bound and continuum states. Our results are in an excellent agreement with the recent experiments of Shah *et al.* [6], but differ from the other measurements by Pieksma *et al.* [5].

From a methodological point of view, we show that the appropriate ETF's not only exactly cancel the spurious asymptotic behavior of nonadiabatic couplings, but also systematically reduce the size and effective range of most coupling matrix elements. With the ETF-corrected molecular basis, the accurate ionization cross sections can be obtained by a calculation in a small region of configuration space and coordinate space. For H_2^+ system in the range 0.1–10 keV/amu, a good convergence has been achieved with a basis including 10 bound states and 11 continuum partial waves.

In addition, we find that the upper levels play a completely different role in g and u components. In case of g components, an excitation sequence via upper levels is the dominant mechanism for the ionization, which enhances the total ionization cross sections (as compared to the direct ionization process) by more than two times at the collision energy $E = 10$ keV/amu. In case of u components, the excitation to upper levels reduces the total ionization cross section significantly, especially the excitation to $2p\pi_u$ molecular state. Since the total ionization cross section is mainly decided by u components, we conclude here that the upper levels are a ''trap'' on the way of electron going to ionization continuum, in contrast the general recognized ''ladder.'' Using the ETF-modified MOCC method, we have a tool to examine the role of each molecular state in the ionization process in a systematic way. The present method is readily applicable to further physical systems of interest, such as He^{++}/H, p/He^+, or p/Li.

ACKNOWLEDGMENTS

One of us (S.Z.) would like to thank the Japanese Government for support. JSPS support by Grant-in-Aid Grant No. 21602/13/01073 is also gratefully acknowledged (L.P.). This work was supported in part by the Ministry of Education, Science, Sport, Culture and Technology, JSPS, and the National Institute for Fusion Science (L.P. and M.K.).

[1] M. Kimura and N.F. Lane, Adv. At., Mol., Opt. Phys. **26**, 79 (1999).
[2] B.H. Bransden and M.R.C. McDowell, *Charge Exchange and the Theory of Ion-Atom Collisions* (Oxford Science, Oxford, 1992).
[3] H.B. Gilbody, Adv. At., Mol., Opt. Phys. **33**, 149 (1994).
[4] H.B. Gilbody, *Proceedings of 19th International Conference on the Physics of Electronic and Atomic Collisons, British Columbia, Canada*, edited by L.J. Dube, J.B. Mitchell, J.W. McConkey, and C.E. Brion (AIP, New York, 1995), Vol. 360, p. 19.
[5] M. Pieksma, S.Y. Ovchinnikov, J. van Eck, W.B. Westerveld, and A. Niehaus, Phys. Rev. Lett. **73**, 46 (1994).
[6] M.B. Shah, J. Geddes, B.M. Mclaughlin, and H.B. Gilbody J. Phys. B **31**, L757 (1998).
[7] M.B. Shah and H.B. Gilbody, J. Phys. B **14**, 2361 (1981).
[8] M.B. Shah, D.S. Elliot, and H.B. Gilbody, J. Phys. B **20**, 2481 (1987).

[9] N. Toshima, Phys. Rev. A **59**, 1981 (1999).
[10] A. Kolakowska, M.S. Pindzola, and D.R. Schultz, Phys. Rev. A **59**, 3588 (1999).
[11] E.Y. Sidky and C.D. Lin, Phys. Rev. A **65**, 012711 (2001).
[12] V. SethuRaman, W.R. Thorson, and C.F. Lebeda, Phys. Rev. A **8**, 1316 (1973).
[13] W.R. Thorson and J.B. Delos, Phys. Rev. A **18**, 117 (1978); **18**, 135 (1978).
[14] W.R. Thorson and G. Bandarage, Phys. Rev. A **37**, 692 (1988); G. Bandarage and W.R. Thorson, *ibid.* **37**, 716 (1988).
[15] T.G. Winter and C.D. Lin, Phys. Rev. A **29**, 3071 (1984).
[16] B.M. Mclaughlin, T.G. Winter and J.F. McCann, J. Phys. B **30**, 1043 (1997).
[17] W. Fritsch and C.D. Lin, Phys. Rev. A **27**, 3361 (1983).
[18] S.Y. Ovchinnikov and J.H. Macek, *Proceding of 18th International Conference on Physics of Electronic and Atomic Collisions Aarhus*, edited by T. Andersen, B. Fastrup, F. Folkmann, and H. Knudsen (IFA Print, Aarhus, 1993).
[19] M. Pieksma, S.Y. Ovchinnikov, and J.H. Macek, J. Phys. B **31**, 1267 (1998).
[20] W.L. Fite, R.F. Stebbings, D.G. Hummer, and R.T. Brackmann, Phys. Rev. **119**, 663 (1960).
[21] J.B. Delos, Rev. Mod. Phys. **53**, 287 (1981).
[22] W.R. Thorson, M. Kimura, J.H. Choi, and S.K. Knudson, Phys. Rev. A **24**, 1768 (1981).
[23] M. Kimura and W.R. Thorson, Phys. Rev. A **24**, 1780 (1981).
[24] D.R. Bates and T.R. Carson, Proc. R. Soc. London, Ser. A **234**, 207 (1956).
[25] G. Hunter and H.O. Pritchard, J. Chem. Phys. **46**, 2146 (1967).
[26] K. Helfrich and H. Hartmann, Theor. Chim. Acta **16**, 263 (1970).
[27] M. Aubert, N. Bessis, and G. Bessis, Phys. Rev. A **10**, 51 (1974).
[28] L.I. Ponomarev and L.N. Somov, J. Comput. Phys. **20**, 183 (1976).
[29] T.G. Winter, M.D. Duncan, and N.F. Lane, J. Phys. B **10**, 285 (1977).
[30] J. Rankin and W.R. Thorson, J. Comput. Phys. **32**, 437 (1979).
[31] The energy of ejected electrons is explicitely included in the equations of motion via the coupling terms in Eq. (2), whilst the total ionization cross section requires a formal integration over the whole continuum. Therefore, we need to revert to a discrete sampling scheme as described further. Our study and also previous works in literature [30,14] find couplings with continuum states to be generally weak, and the full close-coupled equations (2) can be partitioned into separate groups. Each group contains the strongly coupled symmetry allowed discrete states (cf. Table I) and several partial waves for continuum electron with the same energy; these are coupled by weak radial or angular interactions. Truncation in the partial wave expansion of the continuum electron is based on a rapid decrease of the couplings with the increasing angular momentum number (~ 3 orders of magnitude for ejected electron with $l=5$). Next, we calculate the differential ionization cross sections at a certain set of separate energy points, interpolate these with *B* splines, and finally integrate the spline function over the whole continuum analytically. Thus the convergence in the number of continuum states can be controlled through the convergence of *B*-spline interpolation. Ionization cross sections decrease rapidly with the ejected electron energy increase, and the necessary number of interpolation points derives from the number of *B*-spline terms which can accurately represent this function shape. Logarithm equally spaced mesh points of ejected electron energy were conveniently used in our calculation. The differential cross sections (see Fig. 15) already vary smoothly with free electron energies on the 32 point grid (checked also with 64 and 128 points), yielding converged results with sufficient accuracy from our viewpoint.
[32] J. Rankin and W.R. Thorson, Phys. Rev. A **18**, 1990 (1978).
[33] C.F. Barnett, Oak Ridge National Laboratory Report No. 6086 (unpublished).
[34] T.J. Morgan, J. Stone, and R. Mayo, Phys. Rev. A **22**, 1460 (1980).
[35] D.S.F. Crothers and J.F. McCann, J. Phys. B **16**, 3229 (1983).